

Journal of Materials and Engineering Structures

Research Paper

Enhancing Seismic Resilience of Curved Bridges using Shape Memory Alloy with Rubber Bearings

Anil P. Kalyani [a], ***Devesh P. Soni*** [b,*]

[a] *Research Scholar, Gujarat Technological University, Ahmedabad, India*

[b] *Principal, Sardar Vallabhbhai Patel Institute of Technology Vasad, India*

ARTICLEINFO

Article history :

Received : 29 November 2025

Revised : 9 March 2026

Accepted : 26 March 2026

Keywords:

Curved Bridge

Base-Isolation

Shape Memory Alloys

Elastomeric Rubber Bearing

Non-linear Dynamic

ABSTRACT

Shape Memory Alloys (SMA), owing to their superelastic behavior, play a significant role in improving structural performance during seismic events. This study examines the seismic response of a curved bridge isolated with conventional elastomeric rubber bearings (ERB) and shape memory alloy rubber bearings (SMARB) under different ground motion sets. The bridge model consists of a three-span continuous concrete box girder superstructure supported on piers and abutments. Six recorded earthquake ground motions three near-fault and three far-field were considered. The coupled nonlinear equations of motion for the isolated system were solved in incremental form using Newmark's step-by-step method under biaxial excitation in the Seismostruct environment. Sensitivity analysis was performed by varying damping ratios (10–35%) and isolation periods (1.5–3.0s), with key response parameters including pier torsional moment, force transfer to piers, deck displacement, and isolator displacement. Results indicate that SMARB consistently reduces isolator and deck displacements as well as force transfer to piers compared to ERB, while exhibiting higher torsional moments. Overall, the integration of SMA with conventional rubber bearings proves effective for enhancing seismic resilience of curved bridges, provided that isolation parameters are carefully optimized.

1 Introduction

Bridges play a vital role in surface transportation networks, not only for routine service operations but also for rehabilitation and relief during seismic events. Strategically, bridges often serve as evacuation routes, and their failure can result in significant economic losses and casualties. Past earthquakes have shown that bridges are particularly vulnerable to strong ground shaking due to their substantial mass, limited natural damping, and low ductility. For example, during the 1995 Kobe earthquake, the Fukae Bridge suffered a major collapse, while damage to the Gaoyuan Bridge in the 2008 Wenchuan earthquake disrupted the supply of essential resources and restricted rescue operations. Consequently, bridges are regarded as lifeline structures, making it imperative to enhance their seismic resilience.

* *Corresponding author.*
E-mail address: devesh18@gmail.com

e-ISSN: 2170-127X, (cc) BY-SA

RESEARCH REVIEW of Sciences and Technologies

Base isolation has been widely recognized as an effective technique for mitigating seismic damage. Kunde and Jangid [1] demonstrated that isolating bridges under dynamic loading conditions effectively reduced their seismic response. Liu et al. [2] and Ghosh et al. [3] further confirmed that seismic isolation significantly decreases forces and displacements in bridges. Soni et al. [4] illustrated the effectiveness of double variable frequency pendulums in reducing structural response. However, isolated bridges are susceptible to large isolator displacements during strong earthquakes, which can lead to pounding of the bridge deck. Inadequate separation gaps further increase the risk of damage or even collapse.

To overcome these limitations, the use of smart materials such as Shape Memory Alloys (SMAs) has been proposed. SMAs possess unique recentering capability and exhibit minimal residual displacement after seismic events. Unlike traditional isolators, SMAs can return to their original configuration following deformation due to their superelastic behaviour, thereby reducing residual displacements and mitigating the risk of pounding during aftershocks. Their advanced properties—such as enhanced energy dissipation, self-centring, and adaptive response—address key shortcomings of conventional base isolators. Gur et al. [5] incorporated SMA into elastomeric bearings for buildings and found superior control of seismic response compared to conventional systems. Mishra et al. [6] reported favourable vibration control in bridges equipped with SMA, while Dezfuli and Alam [7] demonstrated improved energy dissipation and resilience by integrating ferrous SMA with smart lead rubber bearings. Recent advancements have further expanded the application of Shape Memory Alloys (SMAs) in bridge engineering, ranging from state-of-the-art reviews to novel device configurations and design frameworks. The seismic response of curved bridges presents additional challenges due to their complex geometry. Curved configurations induce torsional effects and non-uniform load distribution, making them more vulnerable compared to straight bridges [8]. Kataria and Jangid [9] studied curved bridges with elastomeric rubber bearings and highlighted the significant influence of geometry on seismic performance. Hosseini et al. [10] utilized a multi-objective optimization algorithm (NSGA-II) to evaluate three different SMA wire configurations (straight, cross, and double-cross) wrapped around Lead Rubber Bearings (LRB), finding that while double-cross arrangements offered superior displacement reduction, straight configurations provided the best overall performance when considering base shear and acceleration.

Gupta and Ghosh [11] examined curved bridges isolated with lead rubber bearings under bi-directional excitation and varying damping ratios, Billah et al. [12] provided a comprehensive review of SMAs in resilient bridges, categorizing their applications into expansion joints, restrainers, isolators, and dampers, highlighting their effectiveness in reducing residual deformations, Further innovations in SMA-based devices have been proposed to address specific seismic challenges. Zhang et al. [13] investigated a cable-stayed bridge isolated with an SMA-based damping brace (SMA-DB) system, emphasizing the sensitivity of the system's response to environmental temperature changes using a direct differentiation method which simultaneously controlled deck displacement and pier base shear, Zhang et al. [14] developed a novel isolation system combining an SMA-friction isolator with an inertia pendulum (IP-SMAFBI), which effectively tunes the structure's natural period. while Gupta et al. [15] evaluated curved bridges with friction pendulum systems, showing effectiveness in controlling torsional moments. Gao et al. [16] proposed a self-centering energy dissipation brace composed of deformation-amplified SMA wires and a friction device (DASMAFD), demonstrating its ability to minimize vulnerability and residual displacement under near-fault and far-field ground motions. Zhou et al. [17] introduced a seismic resilience-based assessment framework for bridge piers reinforced with SMA bars, utilizing peak and residual drift ratios to optimize SMA usage for target functionality recovery. In a related study, Zhou and Alam [18] presented a reliability-based design optimization methodology, determining the minimum SMA replacement ratio required in plastic hinges to meet specific seismic reliability indices and damage limit states over the bridge's design life. Despite these advancements, the seismic performance of curved bridges isolated with SMA-based bearings remains relatively unexplored.

In view of this, the present study undertakes a detailed numerical investigation of curved bridges isolated with SMARB. The specific objectives of this study are (i) to evaluate the response of a curved bridge under near-fault and far-field ground motions, (ii) to examine the effects of varying isolation periods and damping ratios, (iii) to investigate the seismic behaviour of curved bridges isolated with ERB and SMARB, and (iv) to assess critical response parameters including pier torsional moment, force transfer to piers, bearing displacement, and deck displacement under bi-axial excitations.

2 Modelling of Curved Bridge

For this study, the curved bridge model was adopted from the Federal Highway Administration (FHWA) Seismic Design Course, Design Example No. 6, prepared by BAM/Berger Engineers, and previously used by Ates and Constantinou [19] and Kataria and Jangid [9, 20] (Fig. 1). The bridge is a cast-in-place concrete box girder superstructure consisting of three spans

supported on reinforced concrete columns, with span lengths of 27.25 m, 33.5 m, and 27.25 m, and a deck width of 11.8 m. The intermediate bents comprise rectangular columns with a cross-sectional area of 1.7 m² and a height of 6.4 m above the ground surface. The deck has a 10% horizontal slope, and its geometrical and sectional properties are consistent with those of the original bridge.

The cross-sectional area of the deck and pier are 6.238 m² and 1.7 m², respectively, with corresponding moments of inertia of 2.7074 m⁴ and 0.4094 m⁴. The modulus of elasticity for both the deck and piers is 3.5×10^{10} N/m². The mass density is taken as 2.5×10^3 kg/m³ for both components. The total deck length is 88 m, and the pier height is 6.4 m.

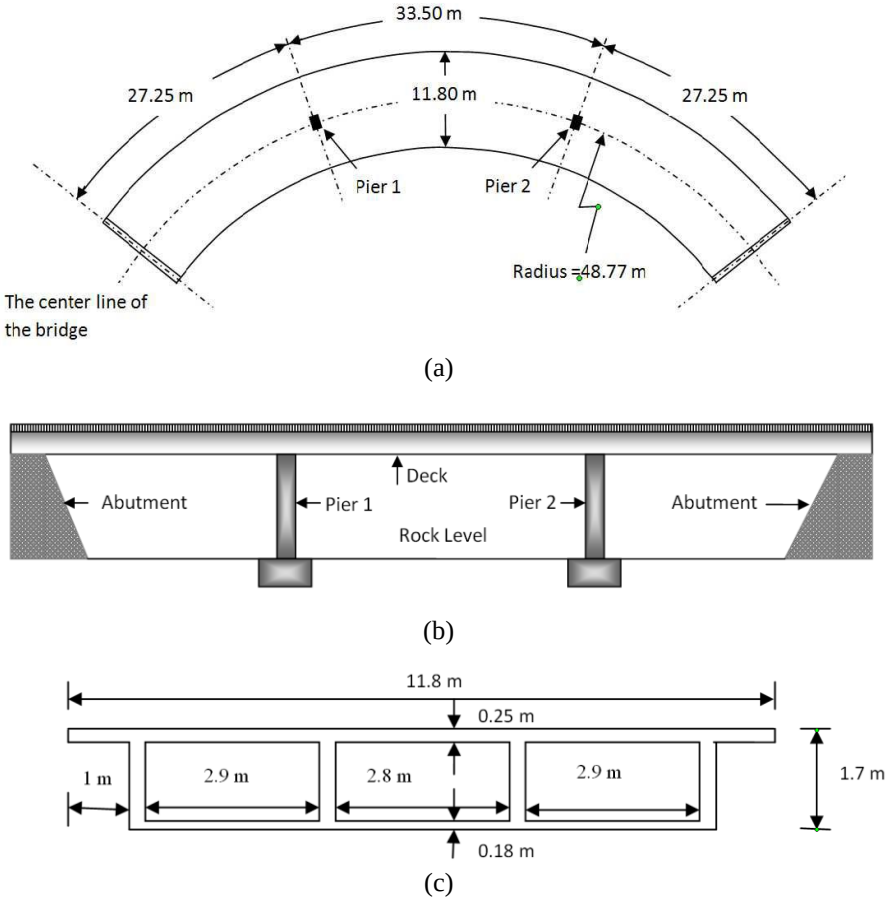


Fig. 1 – (a) Plan of curved bridge (b) Elevation of bridge (c) Section of the superstructure [9]

The bridge is isolated with two bearings at each abutment and pier, resulting in a total of eight bearings positioned directly above the caps of the rectangular columns and abutments. The following assumptions were made for seismic analysis:

1. The curved bridge superstructure and piers are considered elastic under seismic excitation.
2. Soil–structure interaction effects are neglected.
3. Abutments are assumed rigid, while piers are modelled as flexible.
4. The bridge deck is represented as a single spine beam element, with each adjacent element connected by a node.
5. The mass of each element is distributed to the two adjacent nodes in the form of point masses.
6. Non-structural elements, such as parapets and sidewalks, are neglected.

The bridge was modelled using a space frame element as a multi-degree-of-freedom system. Based on detailed design drawings, a three-dimensional analysis model was developed in Seismostruct [21]. Since the central angle of the curved bridge ranges from 12° to 46° between supports, the deck was modelled as a single spine beam consisting of multiple straight beam elements, each with an included angle of less than 3.5°, in accordance with the guidelines of the American Association

of State Highway and Transportation Officials (AASHTO). These specifications are consistent with the load and resistance factor design standards outlined in the National Cooperative Highway Research Program (NCHRP) Report 620 [22]. The pier cap (cap beam) was modelled in Seismostruct as a linear elastic frame element with geometric and material properties consistent with the FHWA benchmark bridge configuration. Flexural and torsional stiffness were calculated based on gross sectional properties. The cap beam was assumed to remain elastic under the considered seismic excitations.

The final finite element model consists of 32 elements for the bridge deck and four elements for the piers. Figure 2 illustrates the mathematical model of the curved bridge with 8 isolators starting from point 34 (IS-1) to point 41 (IS-8)

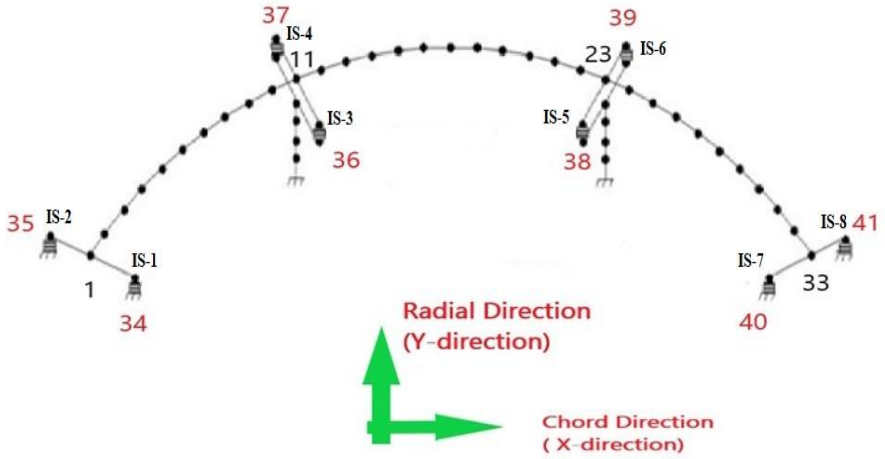


Fig. 2 – Mathematical Model of Isolated Bridge.

2.1 Modelling of ERB

Elastomeric Rubber Bearings (ERBs) are a commonly used isolation system that enhances the seismic performance of structures. They are typically composed of alternating layers of steel and rubber bonded together. During seismic loading, the rubber layers deform to dissipate energy, while the steel plates provide confinement and prevent excessive bulging of the bearing.

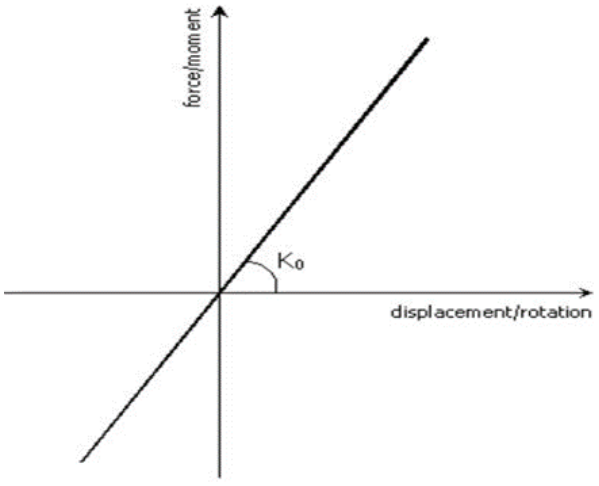


Fig. 3 – Symmetric curve used for modelling of ERB in Seismostruct

In the present study, the ERB is modelled in the Seismostruct environment using a link element with a symmetric linear curve. The symmetric linear curve is widely adopted to represent the idealized linear behaviour of soil foundations and laminated rubber bearings. For this modelling approach, only a single parameter - the initial stiffness (K0) - is required to define the bearing.

In the curved bridge model, isolation bearings are placed at eight locations (points 34 to 41 in Figure 2). The computed properties required for modelling the elastomeric bearings in Seismostruct are summarized in Table 1, corresponding to an isolation period, T_b=2.0 sec and a damping ratio, ζ=0.15.

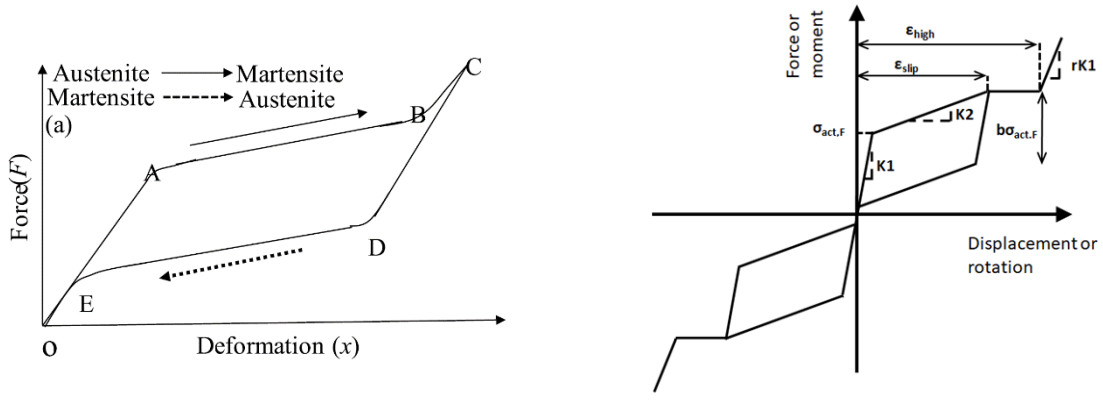
Table 1 -: Properties of elastomeric rubber bearing in Seismostruct.

Bearing location	Mass supported m (kg)	Bearing Stiffness K_o (N/m)	Damping Coefficient c (kg/s)
34 and 40 (A1)	80388.8	793406	75764.7
35 and 41 (A2)	63833.6	630012	60161.7
36 and 38 (P1)	252155	2488666	237650
37 and 39 (P2)	289554	2857783	272898

2.2 Modelling of SMA

Shape Memory Alloys (SMAs) possess the unique property of super elasticity, which allows them to dissipate energy effectively and enhance structural performance during seismic events. In numerical modelling, SMAs can be represented either as truss elements or link elements in Seismostruct. In the present study, SMA is modelled as a link element, incorporating the behavior of a self-centering brace. A link element is essentially a zero-length element defined in terms of force/moment versus displacement/rotation relationships.

Figure 4 (a) illustrates the phase transformation of SMAs from austenite to martensite and back to austenite, while Figure 4 (b) depicts the characteristic hysteresis behavior of self-centering brace type link element highlighting the material's energy dissipation capability. The properties of the Shape Memory Alloy Rubber Bearing used in this study are summarized in Table 2, corresponding to an isolation period of T_b=2.0 sec and a damping ratio of ζ=0.15. K_1 and K_2 are pre- and post-yield stiffness of SMA; K_r is the stiffness of rubber and Kb is the stiffness of SMARB. Damping is incorporated using dashpot elements in Seismostruct. For computing properties to model SMA in Seismostruct, the parameters adopted are: normalized force F_0=0.075, post- to pre-yield stiffness ratio α=0.1, yield displacement u_{ys}=0.025 m, b=1, r=0, and $\varepsilon_{high}=\varepsilon_{slip}$, as shown in Figure 4.1(b).



(a) (b)

Fig. 4 – (a) Phase transformation behavior of SMA [5], (b) Hysteresis curve of SMA [22].

Table 2 -: Properties of shape memory alloy rubber bearing for Seismostruct.

Bearing location	K_1 (SMA) (N/m)	K_2 (SMA) (N/m)	K_r (Rubber) (N/m)	K_b (SMARB) (N/m)
34 and 40 (A1)	1878622	187862.2	442149.8	630012
35 and 41 (A2)	2365843	236584.3	556821.7	793406
36 and 38 (P1)	8521573	852157.3	2005625.7	2857783
37 and 39 (P2)	7420909	742090.9	1746575.1	2488666

3 Numerical Study

The seismic response of the curved bridge equipped with SMARB and ERB was investigated under biaxial components of six recorded earthquake ground motions, consisting of three near-fault and three far-field events. The details of the selected earthquakes are shown in Table 3. For both types of earthquakes, east–west component was applied in the chord direction (x-axis), while the north–south component was applied in the radial direction (y-axis).

Herein, it is to note that in the case of uniaxial loading, earthquake excitation is applied in a single horizontal direction (either chord or radial), resulting in predominantly planar structural response. The induced torsional effects arise mainly due to geometric eccentricities and stiffness irregularities of the curved bridge. In contrast, biaxial loading involves simultaneous application of both horizontal components of earthquake ground motion. This produces coupled translational and torsional response and represents a more realistic seismic excitation condition, particularly for three-dimensional bridge systems. Since the bridge in the present study is a curved configuration modelled as a full three-dimensional structure, biaxial excitation captures more realistic response considering multi-directional seismic effects in curved bridge analysis. Therefore, biaxial loading is considered in the present study.

To enable a direct comparison between the SMARB and ERB systems, the following response parameters were evaluated: pier torsional moment, force transfer to pier, isolator displacement, and deck displacement. To further investigate the effectiveness of the isolation systems, a sensitivity study was performed by varying the damping ratio from 10% to 35% and the isolation period from 1.5 s to 3.0 s.

Table 3 -: Details of near-fault and far-field earthquake ground motions considered.

Sr No.	Earthquake	Station	Component	PGA(g)	Magnitude	Ground motion
1	Loma Prieta (1989)	LGPC	N00E (Chord direction)	0.559	6.93	Near- fault
			N90E (Radial direction)	0.596		
2	Northridge (1994)	SYLMAR	N90S (Chord direction)	0.593	6.9	
			N360S (Radial direction)	0.827		
3	Kobe (1995)	KJMA	KJM000 (Chord direction)	0.63	6.9	
			KJM090 (Radial direction)	0.818		
4	Imperial valley (1940)	117 El Centro # Array 9	I-ELC180 (Chord direction)	0.31	7	Far-field
			I-ELC270 (Radial direction)	0.21		
5	Landers (1992)	Bakers	BAK140 (Chord direction)	0.12	7.35	
			BAK050 (Radial direction)	0.10		
6	Tabas (1978)	Ferdows	EW (Chord direction)	0.09	7.28	
			NS (Radial direction)	0.06		

Figures 5 and 6 present the variation of pier torsional moment with respect to damping ratio for a curved bridge subjected to the near-fault and far-field earthquakes, respectively. The results show that incorporating shape memory alloy (SMA) in rubber bearings increases the pier torsional moment compared to the conventional rubber bearings. The mean value of percentage increase in pier torsional moment of SMARB isolation system compared to the ERB system is shown in Figure 7. The figure shows that at relatively shorter isolation periods (1.5–2.0 s), the increase ranges from 0–50% for near-fault and 0-10% for far field, whereas at longer isolation periods (2.5–3.0 s), the increase ranges from 30-70% and 0-10% for near-fault and far-field ground motions as shown in figure 7. ERB consistently is on reduction side as compared to SMARB, this trend of SMA-based bearings producing higher torsional moments remains consistent across all near-fault and far-field earthquakes. The increase is attributed to the additional stiffness of the SMA in the SMARB and the recentering force of the SMA, which, instead of dissipating torsional energy, transfers larger restoring moments to the piers. However, for isolation periods greater than 3 s, the increase becomes more significant, particularly at lower damping ratios (10–30%), compared to conventional elastomeric rubber bearings for near-fault earthquake.

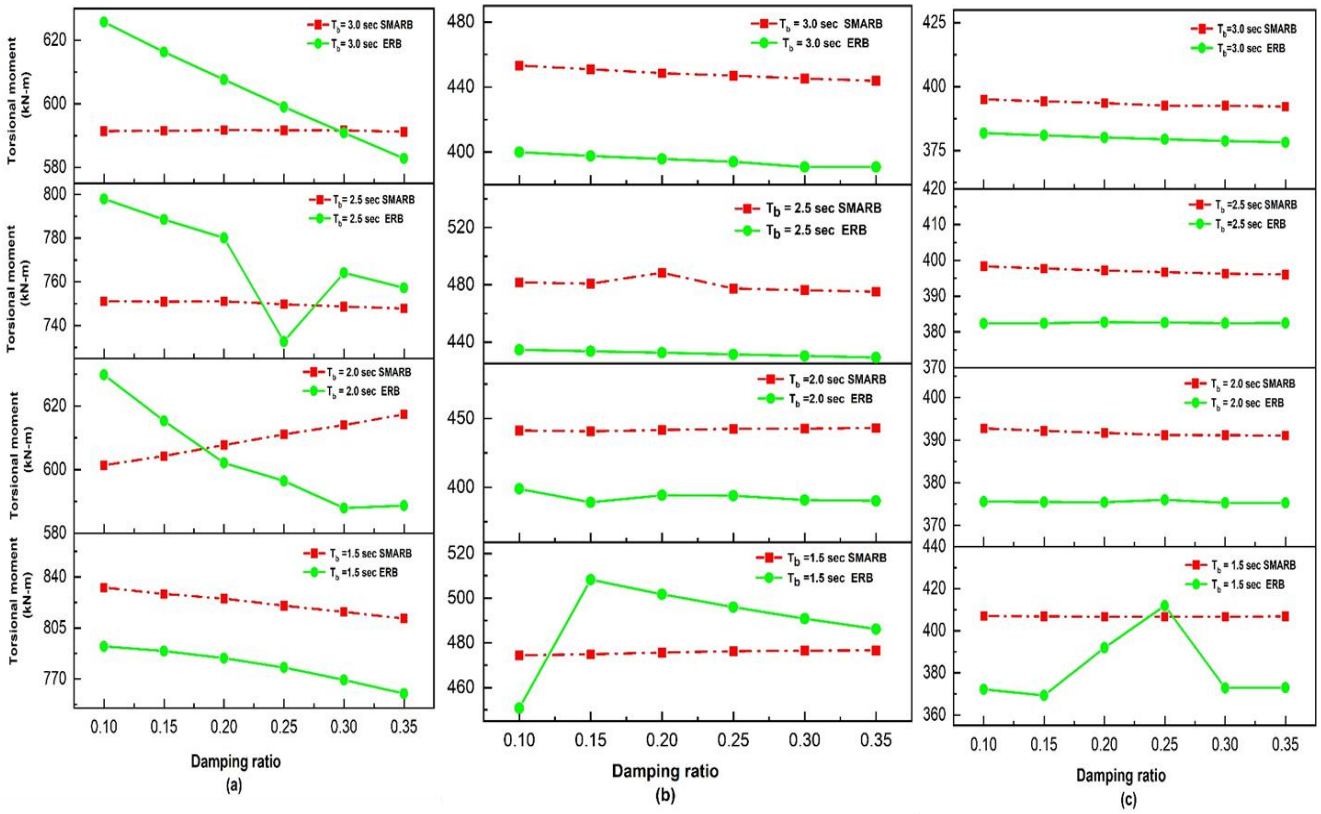


Fig. 5 – Influence of damping ratio of isolation system, ERB and SMARB, on torsional moment under (a) Loma Prieta (1989) (b) Northridge (1994) and (c) Kobe (1995) Earthquakes

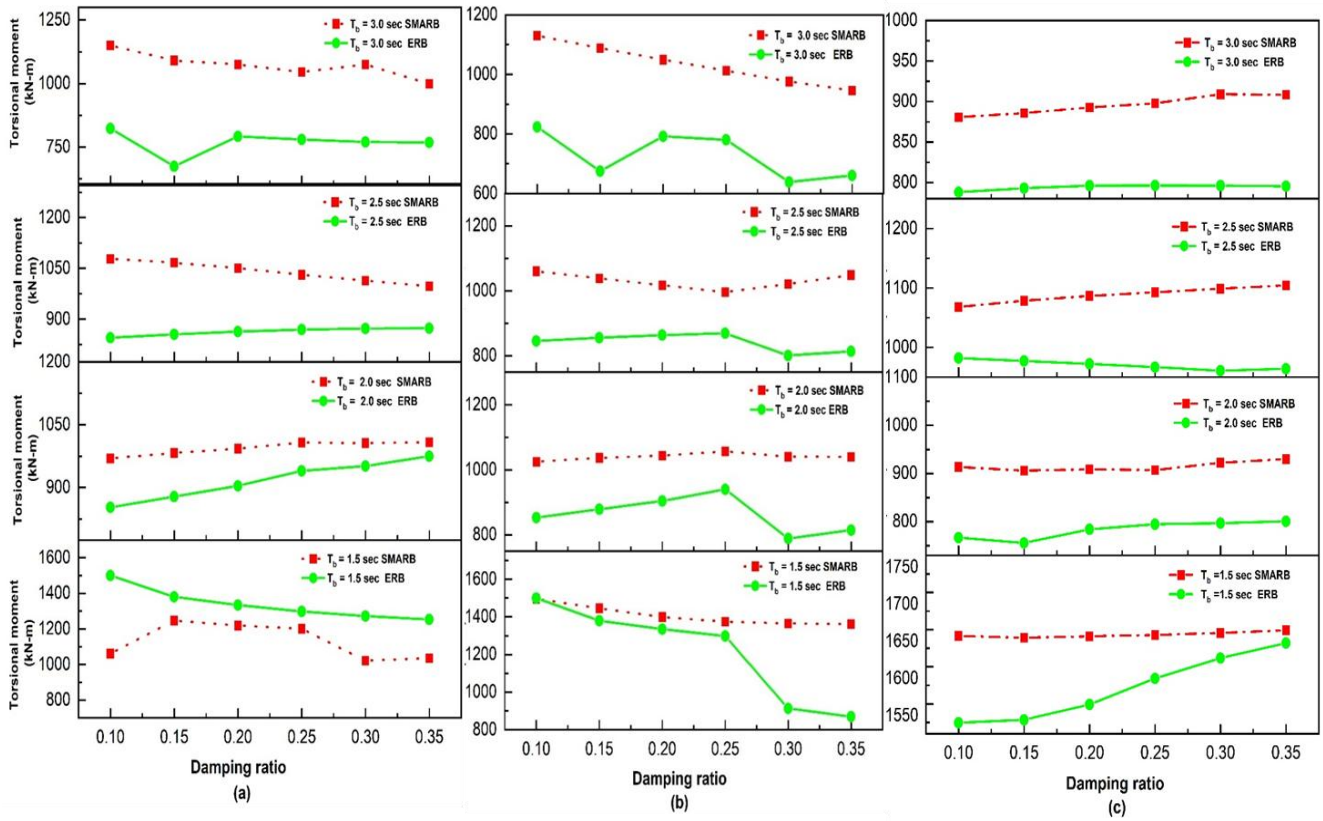


Fig. 6 – Influence of damping ratio of isolation system, ERB and SMARB, on torsional moment under and (a) Imperial valley (1940) (b) Bakers (1992) and (c) Tabas (1978) Earthquakes

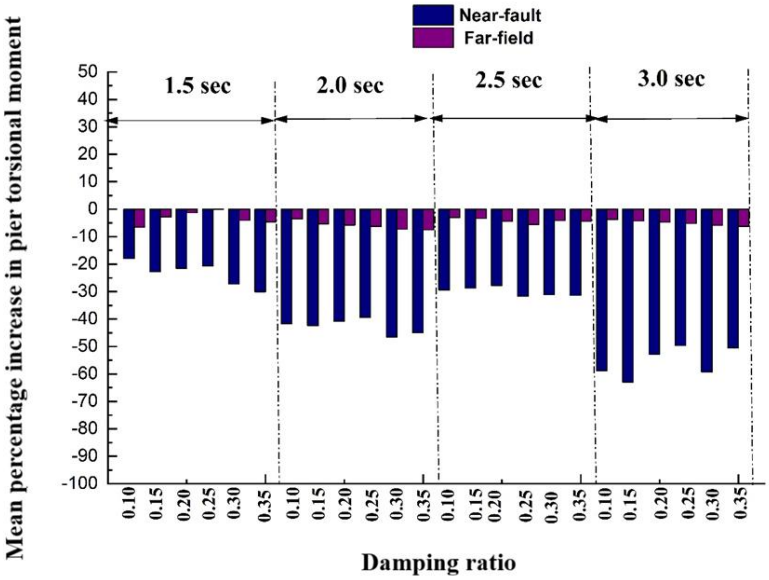


Fig. 7 – Mean percentage difference in pier torsional moment of SMARB isolated bridge compared to the ERB isolated bridge.

Force transfer to piers decreases with increase in damping ratio for both shape memory alloy rubber bearing and elastomeric rubber bearings as shown in Figures 8 and 9 for near-fault and far-field ground motions, respectively. For this study, the calculation of force transfer to the pier was carried out at joint number 11. In the case of shape memory alloys (SMA), the stress–strain behaviour is characterized by a flag-shaped hysteresis loop, which dissipates energy through phase transformations (austenite ↔ martensite).

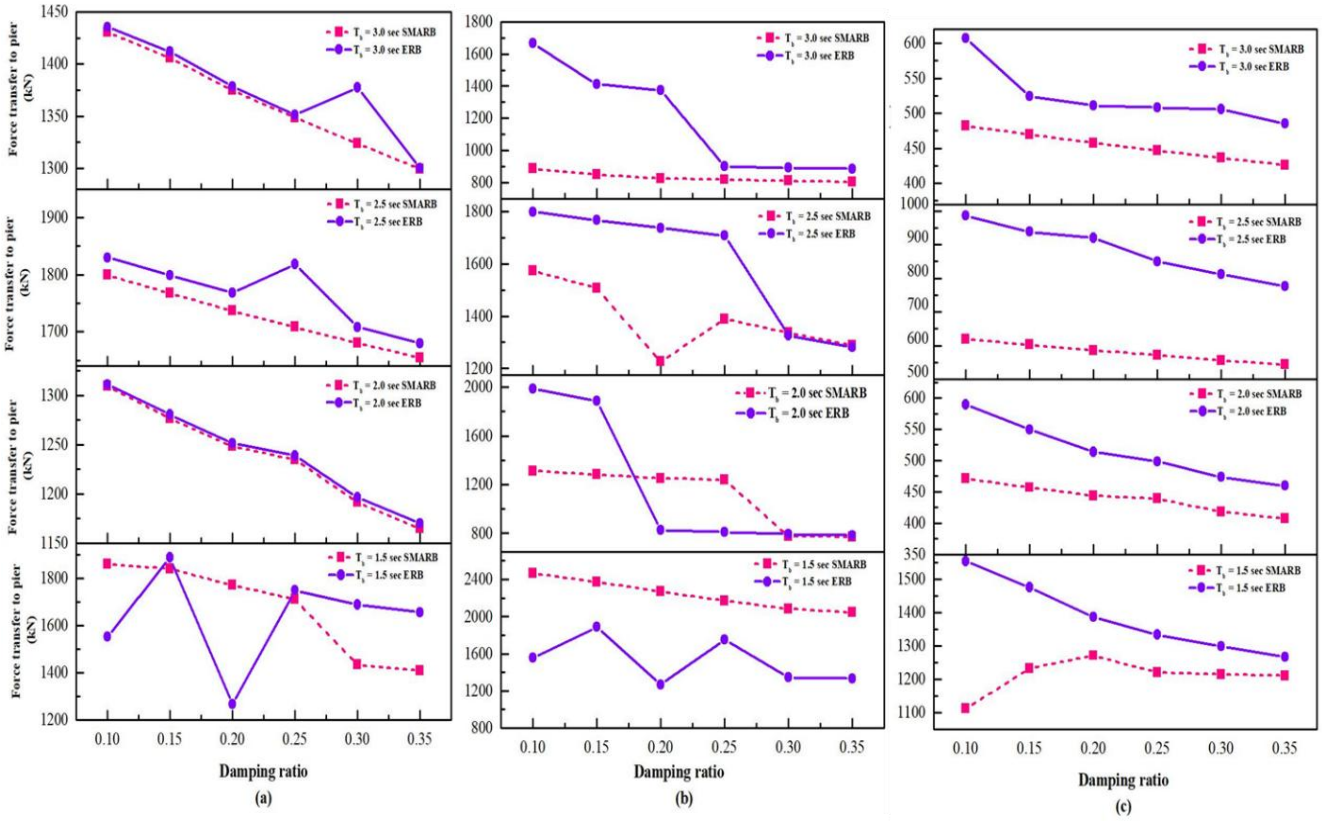


Fig. 8 – Influence of damping ratio of isolation system, ERB and SMARB, on force transfer to pier under (a) Loma Prieta (1989), (b) Northridge (1994) Earthquake and (c) Kobe (1995)

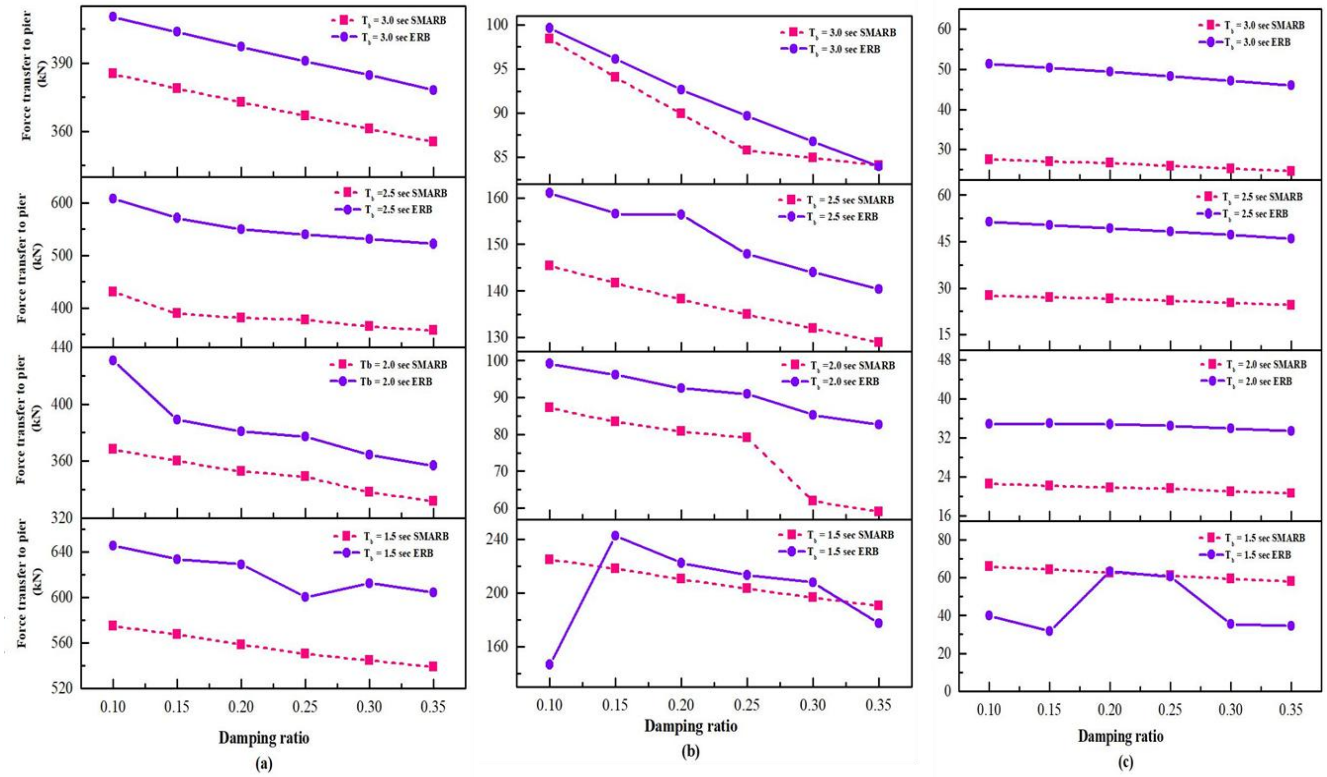


Fig. 9 – Influence of damping ratio of isolation system, ERB and SMARB, on force transfer to pier under (a) Imperial valley (1940) Earthquake, (b) Bakers (1992) and (c) Tabas (1978) Earthquake

Figure 10 presents mean percentage reduction in the forces transfer to pier in SMARB compared to ERB. The reduction in force transfer is found up to 40% for near-fault and up to 20% for far-field ground motions. At longer isolation periods (3.0 s), this reduction is more significant compared to shorter isolation periods (1.5 s). Overall, SMARB consistently transfers lower forces than ERB, highlighting its superior energy-dissipating and recentering capabilities.

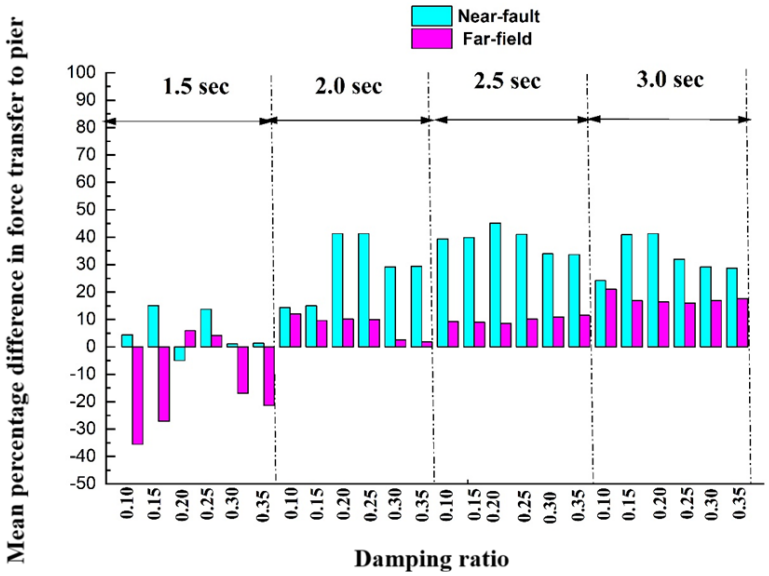


Fig. 10 – Mean percentage reduction (+ve) in force transfer to pier for SMARB isolation system compared to ERB

For curved bridges, large lateral displacements can induce deck rotation and outward movement, increasing the risk of unseating from supports. Reducing isolator displacement helps maintain deck stability and alignment relative to the piers, thereby preventing this unsafe condition. Under bi-axial loading, the maximum bearing displacement occurs at 10% damping; however, for near-fault and far-field earthquakes under consideration, SMARB reduces bearing displacements by 35% to 50%, as shown in Figures 11 and 12.

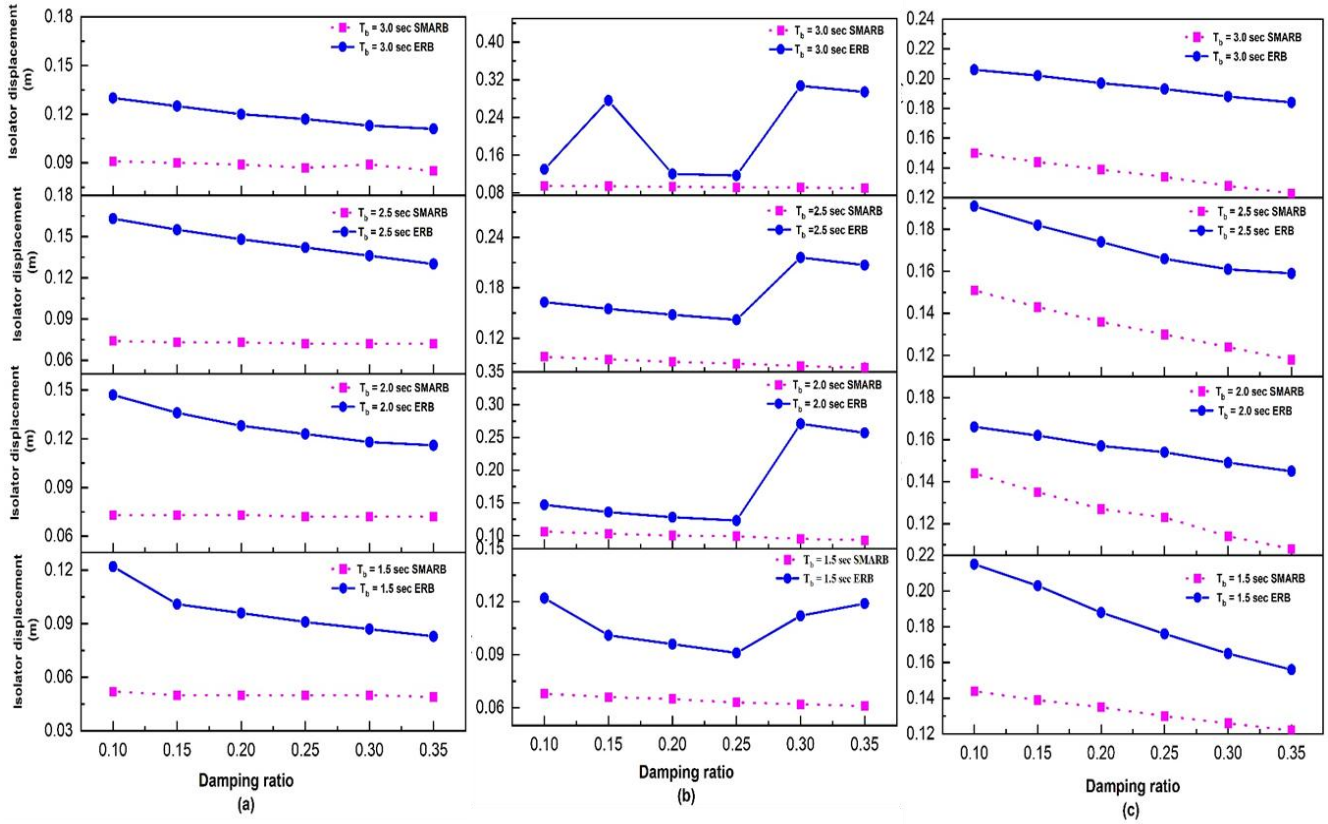


Fig. 11 – Influence of damping ratio of isolation system, ERB and SMARB, on isolator displacement under (a) Loma Prieta (1989), (b) Northridge (1994), and (c) Kobe (1995) Earthquakes

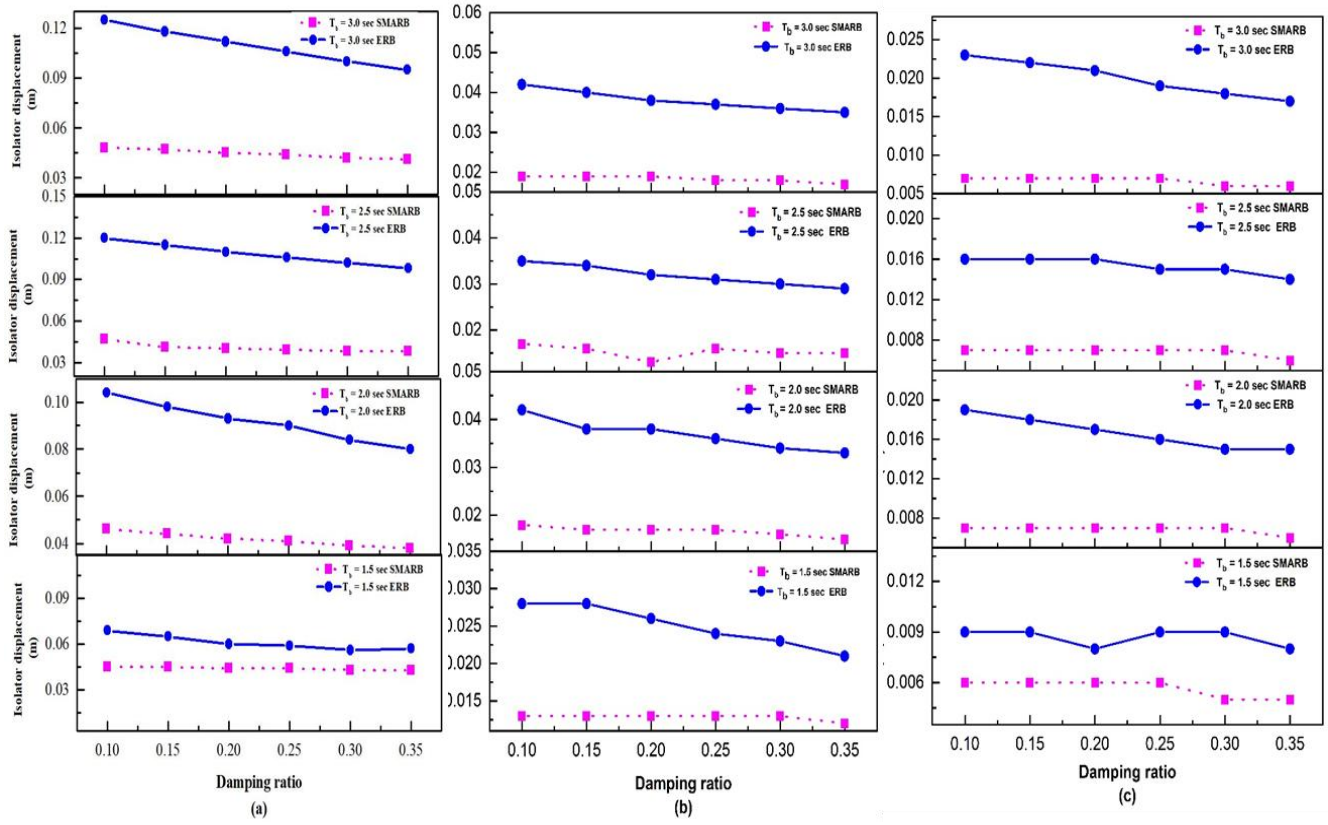


Fig. 12 – Influence of damping ratio of isolation system, ERB and SMARB, on isolator displacement under (a) Imperial valley (1940) (b) Bakers (1992) and (c) Tabas (1978) Earthquake

Figure 13 portrays mean percentage reduction in isolator displacement of bridge with SMARB compared to the ERB. SMARB reduces isolator displacements up to 50% for near-fault and up to 60% for far-field ground motions. These findings demonstrate that while SMA-based bearings effectively reduce bearing displacements, their influence on pier torsional moments and force transfer varies.

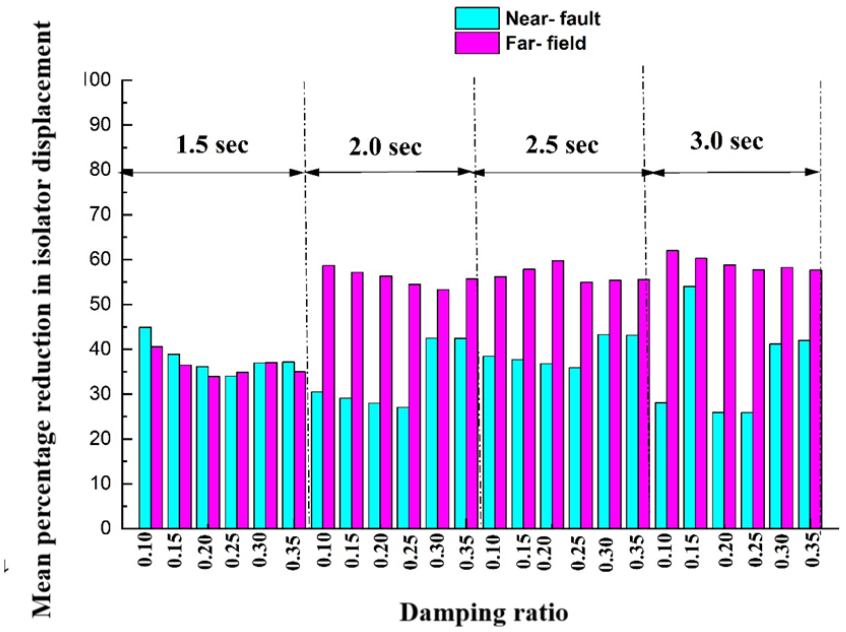


Fig. 13 – Mean percentage reduction in isolator displacement for SMARB isolation system Compared to ERB

Deck displacement is important parameter which is directly linked with life span of structure and unseating of bridges. Figure 14 and 15 illustrates variation of damping effect on deck displacement under bi-axial seismic loading for curved bridge isolated with SMARB and ERB.

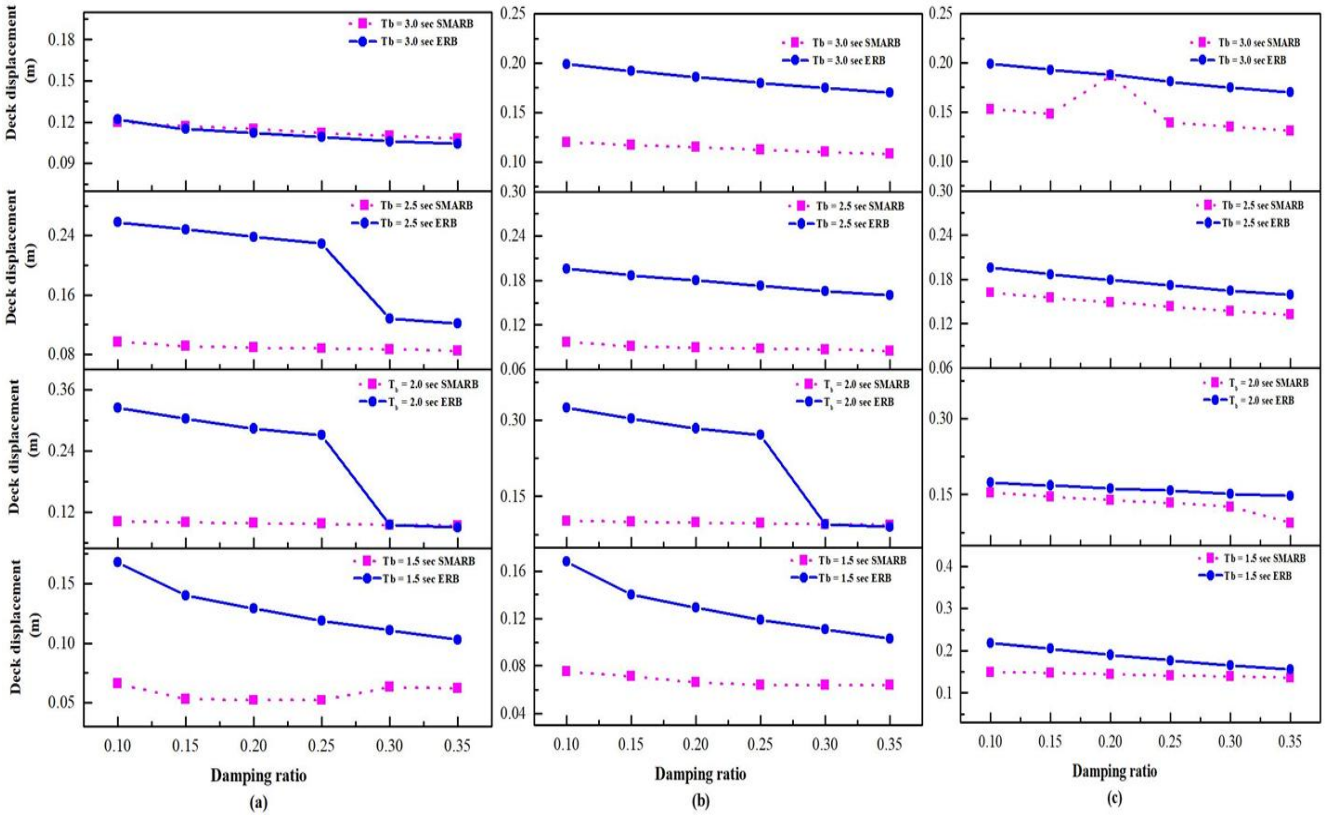


Fig. 14 – Influence of damping ratio of isolation system, ERB and SMARB, on deck displacement under (a) Loma Prieta (1989), (b) Northridge (1994) (c) Kobe (1995) Earthquakes

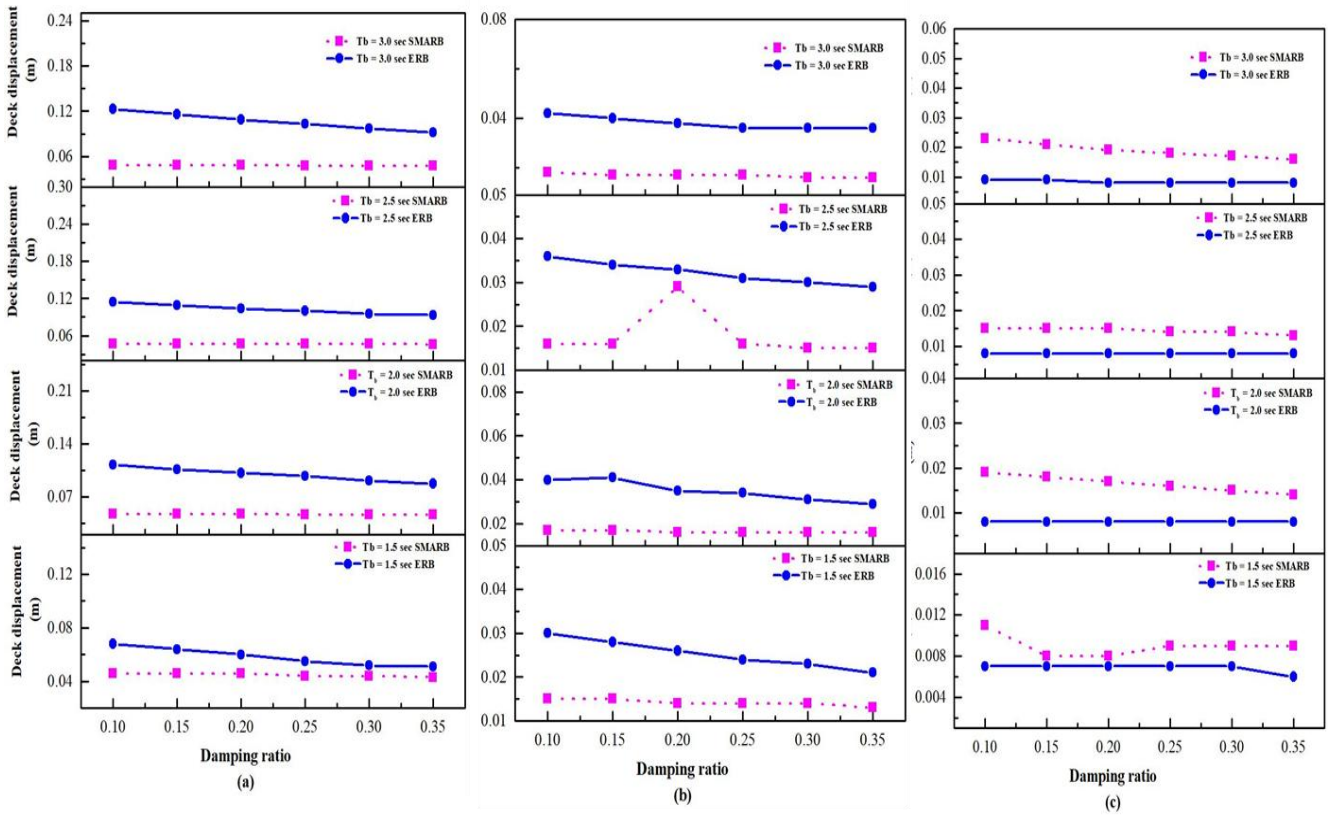


Fig. 15 – Influence of damping ratio of isolation system, ERB and SMARB, on deck displacement under (a) Imperial valley (1940), (b) Bakers (1992) and (c) Tabas (1978) Earthquake

It is observed that the maximum deck displacement occurs at 10% damping; however, incorporating SMA reduces this displacement by nearly half compared to bridges with only rubber bearing. Figure 16 shows mean percentage reduction in deck displacement with varying damping and isolation period for SMARB relative to the ERB. Near-fault ground motion experiences reduction of 20-40% whereas far-field has reduction of 30-60% for bridge with SMARB. This result indicates that addition of shape memory alloys reduces drift in bridge and brings overall stability as compared to conventional mode of isolation.

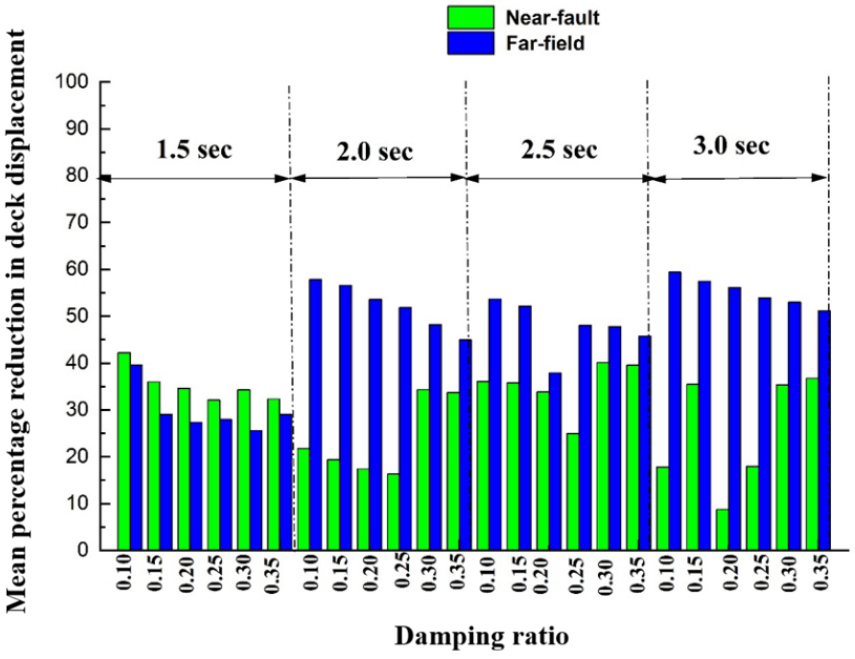


Fig. 16 – Mean percentage reduction in deck displacement of SMARB system compared to ERB system

While SMARB significantly reduces isolator and deck displacements, it results in increased torsional moments in the piers due to the additional stiffness and recentering force provided by the SMA component. From a structural design perspective, this represents a performance trade-off. Excessive isolator displacement in curved bridges may lead to pounding or unseating of the deck, which can cause immediate loss of functionality. In contrast, increased torsional demand in piers can be accommodated through appropriate reinforcement detailing and capacity design principles. Therefore, the observed increase in torsional moment should not be interpreted as a deficiency of the system but rather as a consequence of enhanced stiffness and recentering behavior. Proper optimization of damping ratio and isolation period can further balance torsional demand and displacement control, leading to an efficient seismic isolation strategy.

3.1 Response Sensitivity

Sensitivity analysis is a technique used to evaluate the influence of different factors—such as damping properties, material constants, and geometric parameters—on structural responses. Performing such an analysis helps in understanding structural behavior and provides insights for future design improvements. In the present study, the variations in the peak response of the bridge were examined over a selected range of bearing design parameters. Specifically, the damping ratio and isolation period were varied to identify the conditions that produce the maximum response in the parameters considered. The isolation period corresponds to the effective fundamental period of the isolated bridge system and is governed by the effective stiffness of the isolation devices. It is calculated based on the relationship between participating mass and effective lateral stiffness of the isolation system.

Table 4 - Time period and damping ratio for different cases of isolation system.

Case	Time period (sec)	Damping (%)	Case	Time period (sec)	Damping (%)
1	1.5	10	**13**	2.5	10
2	1.5	15	**14**	2.5	15
3	1.5	20	**15**	2.5	20
4	1.5	25	**16**	2.5	25
5	1.5	30	**17**	2.5	30
6	1.5	35	**18**	2.5	35
7	2.0	10	**19**	3.0	10
8	2.0	15	**20**	3.0	15
9	2.0	20	**21**	3.0	20
10	2.0	25	**22**	3.0	25
11	2.0	30	**23**	3.0	30
12	2.0	35	**24**	3.0	35

Although the present study highlights the sensitivity of seismic response to isolation period and damping ratio, it does not incorporate a formal multi-objective optimization framework. The objective of this work is to establish performance trends and evaluate the comparative effectiveness of SMARB and ERB systems through parametric analysis under recorded ground motions. The development of an integrated optimization methodology considering structural safety, serviceability, torsional demand, displacement control, and economic cost constitutes a broader research direction. Future studies may employ multi-objective optimization algorithms to identify optimal isolation parameters based on performance-based seismic design criteria

Based on the variations in isolation period and damping ratio, a total of 24 cases were analysed as listed in Table 4 and the results are shown in Figures 17 to 20. The responses under near-fault ground motions are shown in part (a) and (c) whereas those under far-field ground motions are depicted in part (b) and (d). Figure 17 illustrates the variation of isolation period and damping ratio with torsional moment for both types of earthquakes. Similarly, Figures 18 and 19 present the variation of force transfer to the pier and isolator displacement, while Figure 20 shows the deck displacement for the different cases.

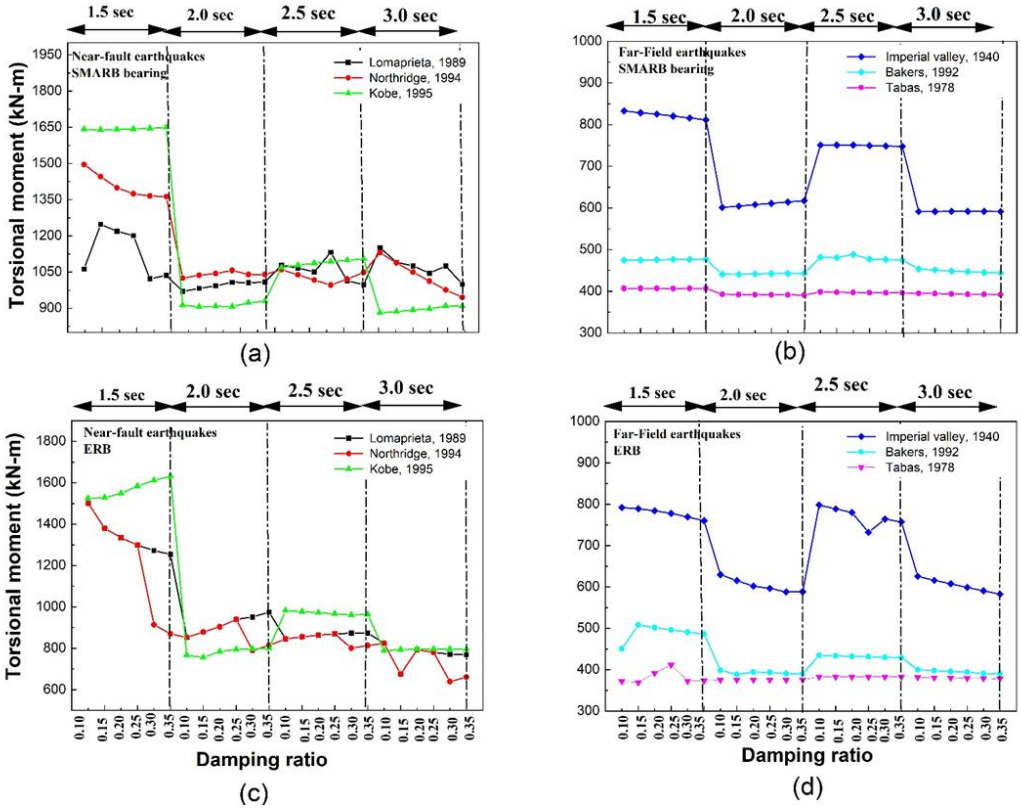


Fig. 17 – Pier torsional-moment response of the curved bridge isolated with SMARB (a) and (b); ERB (c) and (d), evaluated over varying damping ratios and isolation periods

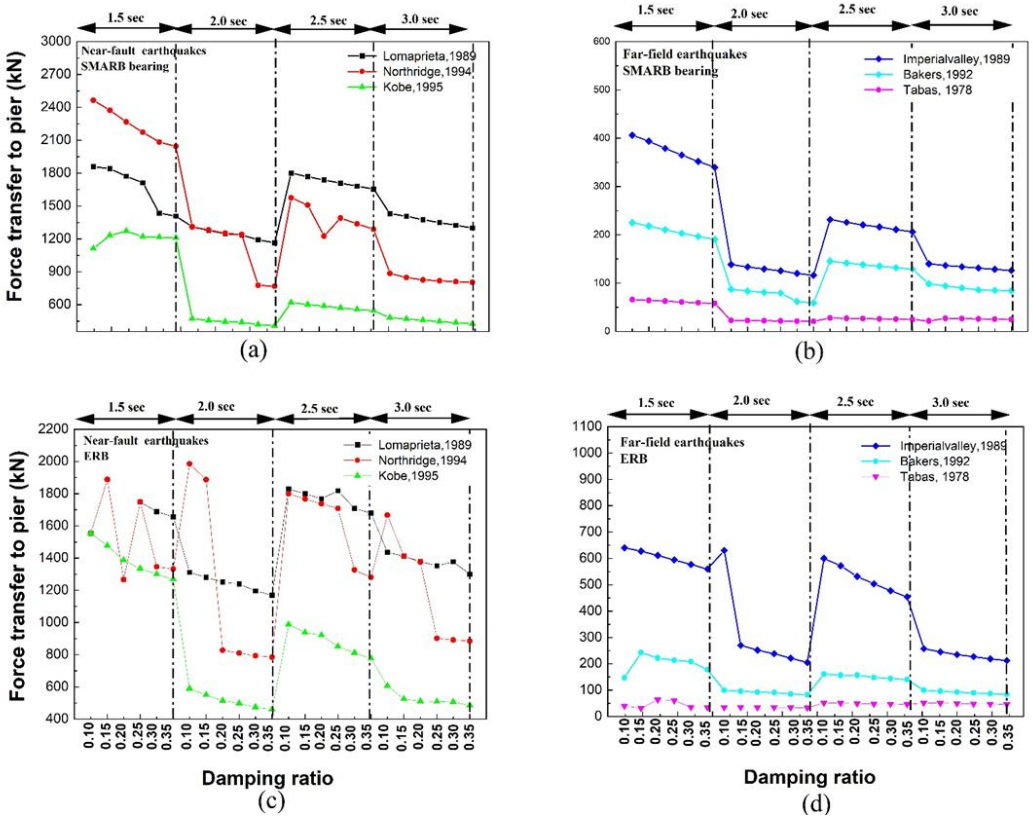


Fig. 18 – Force transfer to pier response of the curved bridge isolated with SMARB (a) and (b); ERB (c) and (d), evaluated over varying damping ratios and isolation periods

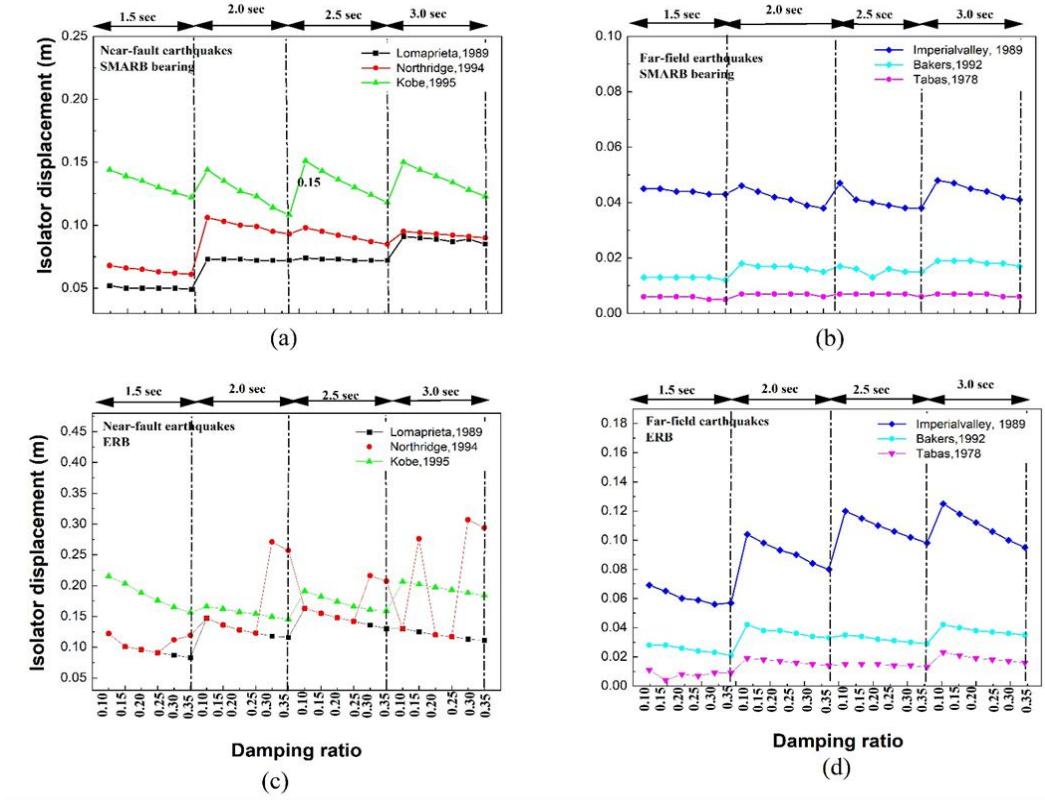


Fig. 19 – Isolator displacement response of the curved bridge isolated with SMARB (a) and (b); ERB (c) and (d), evaluated over varying damping ratios and isolation periods

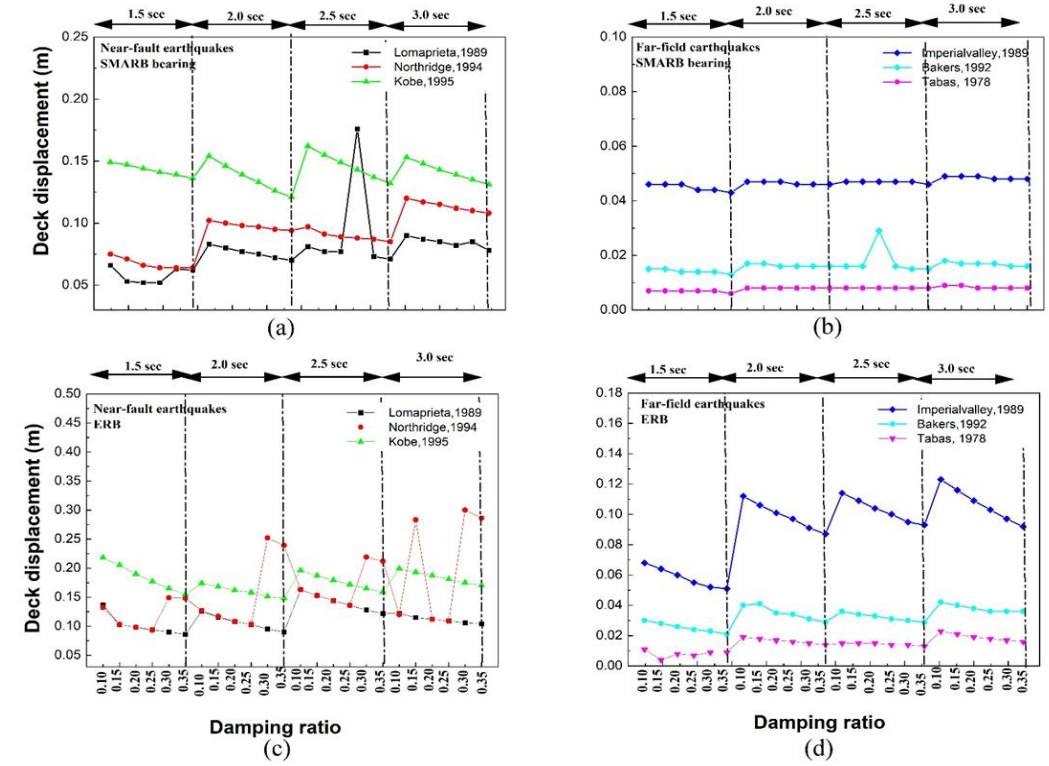


Fig. 20 – Deck displacement response of the curved bridge isolated with SMARB(a) and (b); ERB (c) and (d), evaluated over varying damping ratios and isolation periods

The results indicate that torsional moments are generally higher for the bridge isolated with SMARB compared to ERB. With increasing damping ratio, the force transfers to the pier decreases, whereas isolator displacement reaches its maximum at 10% damping and its minimum at 35% damping. Furthermore, the bridge isolated with SMARB exhibits a significant reduction in deck displacement up to 50% lower compared to the conventional ERB system. The numerical values of sensitivity analysis with varying damping ratio and isolation period with respect to pier torsional moment, force transfer to the pier, isolator displacement, and deck displacement are listed in Appendix A, Tables A1 to A8.

Tables A1 and A2 represents pier torsional moment for curved bridge isolated with ERB and SMARB respectively, responses are evaluated under varying isolation period ranges from (1.5 to 3 Seconds) and damping ratio's (10% to 35 %) under near fault (i.e Loma Prieta, Northridge, Kobe) and far fault (i.e Imperial valley, Bakers and Tabas) earthquakes. It is evident from both the tables that near fault earthquake experiences higher pier torsional moment as compared to far-fault ground motions due to high velocity pulse for example Kobe earthquake consistently yield maximum value across majority of cases with increase in isolation period generally decrease torsional moment for both isolation types. SMARB experiences higher torsional moment as compared to ERB in near fault and far fault earthquakes, for example, at a 1.5s isolation period and 10% damping under the Kobe earthquake, the SMARB yields a torsional moment of 1641.54 kN-m, compared to 1524.72 kN-m for ERB.

Force transfer to pier is depicted in Table A3 for ERB system and Table A4 for SMARB under near and far fault seismic events with varying isolation period and varying damping ratios. From values shown in table it is clear that with increasing damping ratio from 10 % to 35 % FTP reduces for both type of isolation systems but in comparison to ERB; Shape Memory Alloy Rubber Bearing reduces force transfer to pier significantly to 1053.51 kN from 1859.07 kN for Loma Prieta near-fault earthquake with isolation period 1.5 seconds and 10 % damping. Overall trend remains same for majority of earthquakes which highlights energy dissipation capabilities of SMARB over conventional isolation system.

Tables A5 and A6 illustrates results of isolator displacements for the curved bridge equipped with Elastomeric Rubber Bearings (ERB) and Shape Memory Alloy Rubber Bearings (SMARB), respectively. The responses are evaluated across varying isolation periods (1.5 to 3.0 seconds) and damping ratios (10% to 35%) under records of near-fault (Loma Prieta, Northridge, Kobe) and far-field (Imperial Valley, Bakers, Tabas) ground motions. Comparative analysis of data shows that near-fault earthquakes impose substantially greater displacement demands on the isolators compared to far-fault earthquake. For example, under the ERB system at a 1.5-second isolation period and 10% damping, the near-fault Kobe earthquake have an isolator displacement of 0.215 m, whereas the Far-fault Tabas earthquake results in displacement of 0.009. Most importantly, incorporation of SMARB significantly decreases these isolator displacements in comparison to the ERB system across almost all scenarios. For the near-fault Kobe earthquake as benchmark for this parameter (1.5s period, 10% damping), the SMARB system limits the isolator displacement to 0.144 m, marking a notable reduction from the 0.215 m observed in conventional isolation system ERB, this results indicates that smart isolation (i.e SMARB system) facilitate isolator displacement control, which is key for preventing isolator failure or unseating during severe seismic events.

To further evaluate the response of the bridge, Tables A7 and A8 represents the deck displacements for curved bridge in isolation with ERB and SMARB systems, respectively. Similar to the isolator displacement data, these tables illustrate the responses across the same range of isolation periods (1.5-3.0 secs), damping ratios (10-35%), and ground motions (Near fault and far fault). The trends in deck displacement is quite similar to which is observed in isolator displacement, further emphasizing the severity of near-fault ground motions. However, the main takeaway from data in Tables A7 and A8 is the effectiveness of the SMARB system in mitigating response of excessive superstructure movement by controlling deck displacement as compared to ERB. For example, when subjected to the Kobe earthquake at a 1.5-second isolation period and 10% damping, the deck displacement reaches 0.218 m with the ERB system. In contrast, the same bridge in isolation with SMARB reduces this deck displacement to 0.149 m under the same conditions. Increasing the damping ratio generally yields a slight reduction in deck displacement for both systems, though the primary governing factor remains the choice of isolator. Ultimately, the data confirms that the re-centering properties of the shape memory alloys effectively restrain the global displacement of the bridge deck, thereby protecting expansion joints and adjacent structural elements from pounding damage.

The present study is based on nonlinear numerical simulations and does not include independent experimental validation such as shake-table testing of SMARB-isolated curved bridges. Experimental investigation of such systems requires advanced laboratory facilities and sophisticated instrumentation, which were beyond the scope of this work. However, the SMA behavior adopted in this study is based on the uniaxial phenomenological superelastic constitutive model proposed by Auricchio and Sacco [23], which has been extensively validated through experimental research and is implemented in

Seismostruct for concentric SMA brace modelling. Therefore, the numerical results presented herein are supported by experimentally verified material behavior. Nevertheless, future research should focus on experimental validation of SMARB systems at component and structural levels to further establish their practical applicability and reliability under seismic loading.

4 Conclusion

This paper presents an evaluation of the effectiveness of shape memory alloy rubber bearings (SMARB) for seismic mitigation of curved bridges under different sets of ground motions, using nonlinear dynamic time-history analysis in Seismostruct. In addition, a sensitivity analysis was conducted by varying isolation period and damping for parameters such as force transfer to the pier, pier torsional moment, deck displacement, and isolator displacement. Based on results of the study, the following conclusions are drawn:

- Bridges isolated with shape memory alloy rubber bearings (SMARB) exhibit higher torsional moments compared to conventional elastomeric rubber bearings (ERB). The increase is more pronounced at longer isolation periods (2.5–3.0 s), where torsional moments rise by 50–100% relative to ERB, whereas at shorter periods (1.5–2.0 s) the increase remains moderate 5-50%. This trend is consistent across near-fault earthquakes whereas in case of far fault it is 5-15 %only, primarily due to the additional stiffness and recentering force of the SMA, which transfer greater restoring moments to the piers.
- Force transfer to piers decreases with increasing damping ratio for both SMARB and ERB systems. Compared to conventional isolation ERB, SMARB demonstrates reduced force transfer, with reductions in the range of 40% to 80%. The reduction is more significant at longer isolation periods (2.5–3.0 s).
- Maximum isolator displacement occurs at around 10% damping, while the minimum displacement is observed at higher damping ratios (e.g., 35%). Incorporating SMA significantly reduces isolator displacements—by nearly 18% to 71% for near-field earthquakes and up to 68% for far-field earthquakes. Deck displacement is reduced by nearly 60% when using SMARB compared to ERB, enhancing structural stability and minimizing the risk of deck unseating in curved bridges.
- Sensitivity studies shows that variations in damping ratio and isolation period critically influence seismic response parameters. peak responses occur at lower damping ratios (10%), underlines the importance of carefully selecting isolation parameters during design.
- While SMARB increases torsional moments compared to ERB, it consistently reduces isolator and deck displacements as well as force transfer to piers. These results highlight the dual role of smart material (SMA) providing recentering ability and improved energy dissipation while demanding careful design consideration to mitigate higher torsional effects. SMARB shows promise for enhancing seismic resilience of curved bridges, though optimization of parameters such as damping ratio and isolation period is essential for balancing torsional demand with displacement control.

REFERENCES

[1]- M.C. Kunde, R.S. Jangid, Seismic behavior of isolated bridges: A State-of-the-art review. Electron. J. Struct. Eng., 3(3) (2003) 140-170. https://doi.org/10.56748/ejse.335

[2]- Y. Liu, X.J. Qi, Y.J. Wang, S.G. Chen, Seismic mitigation analysis of viscous dampers for curved continuous girder bridge. Appl. Mech. Mater., 90-93(2011) 1230-1233. https://doi.org/10.4028/www.scientific.net/AMM.90-93.1230

[3]- G. Ghosh, Y. Singh, S.K. Thakkar, Seismic response of continuous bridge with isolation bearings. Proc. Inst. Civ. Eng. Bridge Eng., 164(4) (2011) 211-225. https://doi.org/10.1680/bren.2011.164.4.211

[4]- D.P. Soni, B.B. Mistry, V.R. Panchal, Seismic Isolation of Bridges with Double Variable Frequency Pendulum Isolator. Adv. Struct. Eng., 15(2) (2012) 185-203. https://doi.org/10.1260/1369-4332.15.2.185

[5]- S. Gur, S.K. Mishra, S. Chakraborty, Performance assessment of buildings isolated by shape-memory alloy rubber bearing: Comparison with elastomeric bearing under near-fault earthquakes. Struct. Control Health Monit., 21(3) (2014) 449-465. https://doi.org/10.1002/stc.1576

[6]- S.K. Mishra, S. Gur, K. Roy, S. Chakraborty, Response of bridges isolated by shape memory-alloy rubber bearing.

J. Bridge Eng., 20(10) (2015) 04015001. https://doi.org/10.1061/(ASCE)BE.1943-5592.0000837

[7]- F.H. Dezfuli, M.S. Alam, Smart Lead Rubber Bearings Equipped with Ferrous Shape Memory Alloy Wires for Seismically Isolating Highway Bridges. J. Earthquake Eng., 22(6) (2018) 1042-1067. https://doi.org/10.1080/13632469.2016.1269692

[8]- C.M. Galindo, T. Hayashikawa, J.G. Belda, Damage evaluation of curved steel bridges upgraded with isolation bearings and unseating prevention cable restrainers. In: World Academy of Science, Engineering and Technology, Int. J. Civil Environ. Eng. 3(11) 2009 463–471. https://doi.org/10.5281/zenodo.1059655

[9]- N.P. Kataria, R.S. Jangid, Seismic performance and effect of curved geometry on isolation system in horizontally curved bridge. In: Proceedings of the 2013 World Congres on Advances in Structural Engineering and Mechanics, ASEM13, 8–12 September 2013, Jeju, Korea, pp. 1934-1952.

[10]- R. Hosseini, M. Rashidi, B.D. Bulajić, K.K. Arani, Multi-Objective Optimization of Three Different SMA-LRBs for Seismic Protection of a Benchmark Highway Bridge against Real and Synthetic Ground Motions. Appl. Sci., 10(12) (2020) 4076. https://doi.org/10.3390/app10124076

[11]- P.K. Gupta, G. Ghosh, Effect of Bi-directional excitation on a curved bridge with lead rubber bearing. Mater. Today: Proc., 44 (2021) 2239-2244. https://doi.org/10.1016/j.matpr.2020.12.362

[12]- A.H.M.M. Billah, J. Rahman, Q. Zhang, Shape memory alloys (SMAs) for resilient bridges: A state-of-the-art review. Structures, 37 (2022) 514-527. https://doi.org/10.1016/j.istruc.2022.01.034

[13]- N. Zhang, R. Chang, Q. Gu, Response sensitivity studies of a cable-stayed bridge with shape memory alloy damping system considering temperature effects. Eng. Struct., 244 (2021) 112772. https://doi.org/10.1016/j.engstruct.2021.112772

[14]- Z. Zhang, H. Zhou, H. Qian, L. Wang, Shape-memory alloy-friction isolator enhanced with inertia pendulum for seismic mitigation of bridges. Structures, 45 (2022) 243-256. https://doi.org/10.1016/j.istruc.2022.08.123

[15]- P.K. Gupta, S. Agrawal, G. Ghosh, S. Prasanth, K. Virendra, P. Prabhu, Seismic behaviour of the curved bridge with friction pendulum system. J. Asian Archit. Build. Eng., 24(1) (2025) 267-280. https://doi.org/10.1080/13467581.2023.2292089

[16]- X. Gao, Z. Zhang, C. Zhang, Performance-based seismic design and assessment of double-column bridge bent retrofitted with a novel shape memory alloy-friction brace, 73 (2025) 108331. https://doi.org/10.1016/j.istruc.2025.108331

[17]- L. Zhou, A. Ye, M.S. Alam, Seismic resilience-based assessment and design of bridge piers reinforced with SMA bars. Eng. Struct., 345 Part A (2025) 121420. https://doi.org/10.1016/j.engstruct.2025.121420

[18]- L. Zhou, M.S. Alam, Seismic reliability-based assessment and design optimization of shape memory alloy bars in concrete bridge piers. Eng. Struct., 322 Part B (2025) 119226. https://doi.org/10.1016/j.engstruct.2024.119226

[19]- S. Ates, M.C. Constantinou, Example of application of response spectrum analysis for seismically isolated curved bridges including soil-foundation effects. Soil Dyn. Earthquake Eng., 31(4) (2011) 648-661. https://doi.org/10.1016/j.soildyn.2010.12.002

[20]- N.P. Kataria, R.S. Jangid, Seismic protection of the horizontally curved bridge with semi-active variable stiffness damper and isolation system. Adv. Struct. Eng., 19(7) (2016) 1221-1238. https://doi.org/10.1177/1369433216634477

[21]- SeismoSoft, SeismoStruct Software Version 2022: Earthquake Engineering Software Solutions. A computer program for seismic assessment and retrofitting of RC structures. 2022.

[22]- Transportation Research Board, In: National Cooperative Highway Research Program (NCHRP) Report 620: Development of Design Specifications and Commentary for Horizontally Curved Concrete Box-Girder Bridges. The National Academies Press, 2008. https://doi.org/10.17226/14186

[23]- F. Auricchio, E. Sacco, A one-dimensional model for superelastic shape-memory alloys with different elastic properties between austenite and martensite. Int. J. Non-Linear Mech., 32(6) (1997) 1101-1114. https://doi.org/10.1016/S0020-7462(96)00130-8

Appendix A. Numerical values of sensitivity analysis with varying damping ratio and isolation period

Table A1 -: Pier torsional moment of curved bridge with ERB under near-fault and far-field earthquakes

Isolation period (sec)	Damping (%)	Pier torsional moment (kN-m)					
		Loma Prieta (1989)	Northridge (1994)	Kobe (1995)	Imperial valley (1940)	Bakers (1992)	Tabas (1978)
	10	724.05	1500.36	1524.72	792.40	450.79	372.17
	15	797.56	1380.31	1528.55	789.18	508.30	369.31
1.5	**20**	792.40	1334.52	1549.37	784.29	501.76	391.91
	25	788.27	1298.51	1584.30	777.87	496.01	411.92
	30	785.09	913.73	1611.60	769.37	490.85	372.89
	35	781.94	869.70	1631.95	760.09	486.19	372.99
	10	521.78	852.74	766.93	629.83	398.86	375.56
	15	518.95	878.67	755.89	615.37	389.01	375.47
2	**20**	520.00	904.21	784.29	602.14	394.18	375.40
	25	525.42	940.12	794.60	596.47	393.87	376.00
	30	524.36	788.81	796.92	587.92	390.70	375.27
	35	527.46	814.48	800.72	588.71	390.12	375.26
	10	699.67	845.56	982.16	797.93	434.58	382.39
2.5	**15**	691.37	855.55	977.16	788.51	433.48	382.42
	20	683.48	863.61	972.23	780.11	432.50	382.72
	25	675.84	869.52	966.98	732.87	431.36	382.61
	30	668.64	801.01	960.85	764.15	430.29	382.46
	35	661.56	813.60	964.18	757.26	429.20	382.48
	10	505.83	823.78	788.02	625.73	399.98	381.82
	15	504.93	675.04	793.12	616.30	397.60	380.97
3	**20**	502.38	792.17	796.27	607.66	395.79	380.14
	25	506.32	780.47	796.30	599.04	394.07	379.43
	30	510.18	639.18	796.12	590.91	390.82	378.77
	35	514.04	660.52	795.54	582.84	390.82	378.19

Table A2 -: Pier torsional moment of curved bridge with SMARB under near-fault and far-field earthquakes

Isolation period (sec)	Damping (%)	Pier torsional moment (kN-m)					
		Loma Prieta (1989)	Northridge (1994)	Kobe (1995)	Imperial valley (1940)	Bakers (1992)	Tabas (1978)
	10	1062.15	1495.57	1641.54	832.80	474.46	407.00
	15	1247.38	1445.63	1639.04	828.40	474.86	406.85
1.5	**20**	1219.06	1399.53	1640.91	825.20	475.66	406.76
	25	1201.06	1374.81	1642.97	820.30	476.25	406.70
	30	1022.21	1365.26	1645.45	816.06	476.50	406.72
	35	1036.23	1362.44	1648.99	811.56	476.63	406.89
	10	969.82	1025.00	913.33	601.42	441.31	392.76
	15	982.54	1036.73	905.80	604.29	440.62	392.18
2	**20**	992.95	1043.64	908.75	607.72	441.63	391.72
	25	1007.73	1056.54	916.95	611.08	442.48	391.18
	30	1006.42	1040.20	922.39	614.03	442.67	391.15
	35	1008.44	1040.05	929.99	617.38	443.11	391.09
	10	1078.58	1059.97	1068.22	751.05	481.72	398.37
2.5	**15**	1066.87	1038.10	1078.08	750.95	480.75	397.74
	20	1051.03	1016.84	1086.75	751.06	488.39	397.18
	25	1131.55	996.08	1092.93	749.74	477.42	396.71
	30	1014.19	1020.75	1098.88	748.65	476.27	396.29
	35	997.55	1048.45	1104.44	747.87	475.23	396.07
	10	1150.60	1129.94	880.65	591.39	453.18	395.02
3	**15**	1091.12	1087.95	885.78	591.55	450.97	394.26
	20	1075.12	1049.63	892.73	591.69	448.46	393.55
	25	1045.63	1012.67	897.88	591.66	446.99	392.56
	30	1075.16	976.38	909.09	591.67	445.24	392.56
	35	998.93	945.66	908.43	591.21	443.81	392.21

Table A3 -: Force transfer to pier of the curved bridge with ERB under near-fault and far-field earthquakes

Isolation period (sec)	Damping (%)	Force transfer to pier (kN)					
		Loma Prieta (1989)	Northridge (1994)	Kobe (1995)	Imperial valley (1940)	Bakers (1992)	Tabas (1978)
	10	1859.07	2464.06	1554.06	645.64	224.90	39.97
	15	1840.64	2373.15	1476.12	633.71	242.60	31.81
1.5	**20**	1771.78	2268.42	1386.62	629.09	222.40	63.22
	25	1711.78	2172.12	1334.04	600.20	213.40	60.51
	30	1433.35	2083.87	1299.57	612.43	207.90	35.43
	35	1409.05	2044.92	1267.78	604.45	177.50	34.53
	10	1309.50	1985.04	589.45	430.52	99.23	34.86
	15	1276.76	1886.84	549.57	388.91	96.20	34.98
2	**20**	1248.27	827.95	513.84	380.91	92.55	34.81
	25	1235.01	809.36	498.62	376.99	90.98	34.52
	30	1191.52	793.42	473.41	364.39	85.30	33.96
	35	1164.83	784.17	459.64	356.84	82.67	33.37
	10	1830.03	1573.81	986.74	608.00	161.04	51.40
2.5	**15**	1799.17	1507.85	938.15	571.64	156.60	50.43
	20	1768.43	1225.45	920.16	549.42	156.37	49.36
	25	1818.42	1389.71	850.63	539.90	147.92	48.26
	30	1708.35	1336.74	811.50	530.95	144.02	47.13
	35	1679.64	1288.20	776.03	522.11	140.36	45.98
	10	1435.69	885.35	607.09	410.27	99.64	51.4
3	**15**	1406.27	847.50	524.15	403.62	96.15	50.43
	20	1378.48	825.33	511.12	397.16	92.66	49.36
	25	1351.46	817.67	508.10	390.82	89.71	48.26
	30	1377.49	810.16	505.78	384.65	86.77	47.13
	35	1300.33	803.13	485.20	378.05	45.98	212.00

Table A4 -: Force transfer to pier of the curved bridge with SMARB under near-fault and far-field earthquakes

Isolation period (sec)	Damping (%)	Force transfer to pier (kN)					
		Loma Prieta (1989)	Northridge (1994)	Kobe (1995)	Imperial Valley (1940)	Bakers (1992)	Tabas (1978)
	10	1053.51	1553.36	1111.50	406.17	146.70	65.76
	15	839.60	1888.55	1232.74	393.91	218.20	64.27
1.5	**20**	785.34	1266.65	1271.00	378.91	210.40	62.52
	25	738.09	1749.27	1220.52	364.84	203.20	60.89
	30	696.78	1346.68	1214.75	351.81	196.50	59.36
	35	665.27	1332.77	1210.68	339.60	190.50	57.92
	10	337.29	1311.05	470.92	138.60	87.29	22.55
	15	314.93	1280.70	456.77	133.62	83.38	22.16
2	**20**	295.08	1251.40	443.63	129.26	80.85	21.78
	25	281.34	1238.93	438.79	125.36	79.04	21.59
	30	262.30	776.87	418.34	120.10	61.94	20.99
	35	248.58	768.51	406.57	116.19	59.02	20.60
	10	578.65	1799.26	619.01	231.39	145.43	27.51
2.5	**15**	555.55	1767.42	602.24	225.85	141.71	26.98
	20	534.93	1736.97	586.19	220.53	138.20	26.64
	25	513.89	1708.13	571.58	216.31	134.90	25.90
	30	495.16	1327.01	555.63	210.67	132.00	25.21
	35	477.62	1280.85	543.41	206.05	128.97	24.55
	10	220.52	667.16	481.67	139.88	98.39	21.51
	15	387.87	1412.22	469.58	136.62	94.08	26.98
3	**20**	365.90	1374.67	457.52	133.78	89.92	26.64
	25	346.08	901.92	446.66	131.12	85.77	25.90
	30	327.86	791.60	436.13	128.64	84.93	25.21
	35	311.35	785.02	426.13	126.10	84.10	24.55

Table A5 -: Isolator displacement of the curved bridge with ERB under near-fault and far-field earthquake

Isolation period (sec)	Damping (%)	Isolator displacement (m)					
		Loma Prieta (1989)	Northridge (1994)	Kobe (1995)	Imperial valley (1940)	Bakers (1992)	Tabas (1978)
	10	0.122	0.122	0.215	0.069	0.028	0.009
	15	0.101	0.101	0.203	0.065	0.028	0.008
1.5	**20**	0.096	0.096	0.188	0.060	0.026	0.008
	25	0.091	0.091	0.176	0.059	0.024	0.009
	30	0.087	0.112	0.165	0.056	0.023	0.009
	35	0.083	0.119	0.156	0.057	0.021	0.008
	10	0.147	0.147	0.166	0.104	0.042	0.019
	15	0.136	0.136	0.162	0.098	0.038	0.018
2	**20**	0.128	0.128	0.157	0.093	0.038	0.017
	25	0.123	0.123	0.154	0.090	0.036	0.016
	30	0.118	0.271	0.149	0.084	0.034	0.015
	35	0.116	0.257	0.145	0.080	0.033	0.015
	10	0.163	0.163	0.191	0.120	0.035	0.016
2.5	**15**	0.155	0.155	0.182	0.115	0.034	0.016
	20	0.148	0.148	0.174	0.110	0.032	0.016
	25	0.142	0.142	0.166	0.106	0.031	0.015
	30	0.136	0.216	0.161	0.102	0.030	0.015
	35	0.130	0.207	0.159	0.098	0.029	0.014
	10	0.130	0.130	0.206	0.125	0.042	0.023
3	**15**	0.125	0.276	0.202	0.118	0.040	0.022
	20	0.120	0.120	0.197	0.112	0.038	0.021
	25	0.117	0.117	0.193	0.106	0.037	0.019
	30	0.113	0.307	0.188	0.100	0.036	0.018
	35	0.111	0.294	0.184	0.095	0.035	0.017

Table A6 -: Isolator displacement of the curved bridge with SMARB under near-fault and far-field earthquakes

Isolation period (sec)	Damping (%)	Isolator displacement (m)					
		Loma Prieta (1989)	Northridge (1994)	Kobe (1995)	Imperial valley (1940)	Bakers (1992)	Tabas (1978)
	10	0.052	0.068	0.144	0.045	0.013	0.006
	15	0.050	0.066	0.139	0.045	0.013	0.006
1.5	**20**	0.050	0.065	0.135	0.044	0.013	0.006
	25	0.050	0.063	0.130	0.044	0.013	0.006
	30	0.050	0.062	0.126	0.043	0.013	0.005
	35	0.049	0.061	0.122	0.043	0.012	0.005
	10	0.073	0.106	0.144	0.046	0.018	0.007
	15	0.073	0.103	0.135	0.044	0.017	0.007
2	**20**	0.073	0.100	0.127	0.042	0.017	0.007
	25	0.072	0.099	0.123	0.041	0.017	0.007
	30	0.072	0.095	0.114	0.039	0.016	0.007
	35	0.072	0.093	0.108	0.038	0.015	0.006
	10	0.074	0.098	0.151	0.047	0.017	0.007
2.5	**15**	0.073	0.095	0.143	0.041	0.016	0.007
	20	0.073	0.092	0.136	0.040	0.013	0.007
	25	0.072	0.090	0.130	0.039	0.016	0.007
	30	0.072	0.087	0.124	0.038	0.015	0.007
	35	0.072	0.085	0.118	0.038	0.015	0.006
	10	0.091	0.095	0.150	0.048	0.019	0.007
3	**15**	0.090	0.094	0.144	0.047	0.019	0.007
	20	0.089	0.093	0.139	0.045	0.019	0.007
	25	0.087	0.092	0.134	0.044	0.018	0.007
	30	0.089	0.091	0.128	0.042	0.018	0.006
	35	0.085	0.090	0.123	0.041	0.017	0.006

Table A7 -: Deck displacement of the curved bridge with ERB under near-fault and far-field earthquakes

Isolation period (sec)	Damping (%)	Deck displacement (m)					
		Loma Prieta (1989)	Northridge (1994)	Kobe (1995)	Imperial valley (1940)	Bakers (1992)	Tabas (1978)
1.5	10	0.137	0.132	0.218	0.068	0.030	0.011
	15	0.103	0.103	0.205	0.064	0.028	0.008
	20	0.098	0.098	0.190	0.060	0.026	0.008
	25	0.094	0.093	0.177	0.055	0.024	0.009
	30	0.090	0.149	0.165	0.052	0.023	0.009
	35	0.086	0.148	0.155	0.051	0.021	0.009
2	10	0.126	0.127	0.174	0.112	0.040	0.019
	15	0.115	0.117	0.168	0.106	0.041	0.018
	20	0.108	0.108	0.162	0.101	0.035	0.017
	25	0.103	0.103	0.158	0.097	0.034	0.016
	30	0.095	0.252	0.151	0.091	0.031	0.015
	35	0.090	0.239	0.148	0.087	0.029	0.014
2.5	10	0.163	0.163	0.196	0.114	0.036	0.015
	15	0.153	0.153	0.187	0.109	0.034	0.015
	20	0.144	0.144	0.179	0.104	0.033	0.015
	25	0.176	0.136	0.172	0.100	0.031	0.014
	30	0.128	0.219	0.165	0.095	0.030	0.014
	35	0.122	0.212	0.159	0.093	0.029	0.013
3	10	0.122	0.125	0.199	0.123	0.042	0.023
	15	0.115	0.283	0.193	0.116	0.040	0.021
	20	0.112	0.117	0.188	0.109	0.038	0.019
	25	0.109	0.119	0.181	0.103	0.036	0.018
	30	0.106	0.300	0.218	0.097	0.036	0.017
	35	0.104	0.286	0.205	0.092	0.036	0.016

Table A8 -: Deck displacement of the curved bridge with SMARB under near-fault and far-field earthquakes

Isolation period (sec)	Damping (%)	Deck displacement (m)					
		Loma Prieta (1989)	Northridge (1994)	Kobe (1995)	Imperial valley (1940)	Bakers (1992)	Tabas (1978)
1.5	10	0.066	0.075	0.149	0.046	0.015	0.007
	15	0.053	0.071	0.147	0.046	0.015	0.007
	20	0.052	0.066	0.144	0.046	0.014	0.007
	25	0.052	0.064	0.141	0.044	0.014	0.007
	30	0.063	0.064	0.139	0.044	0.014	0.007
	35	0.062	0.064	0.136	0.043	0.013	0.006
2	10	0.083	0.102	0.154	0.047	0.017	0.008
	15	0.080	0.100	0.146	0.047	0.017	0.008
	20	0.077	0.098	0.139	0.047	0.016	0.008
	25	0.075	0.097	0.133	0.046	0.016	0.008
	30	0.072	0.095	0.126	0.046	0.016	0.008
	35	0.070	0.094	0.121	0.046	0.016	0.008
2.5	10	0.081	0.097	0.162	0.047	0.016	0.008
	15	0.077	0.091	0.155	0.047	0.016	0.008
	20	0.077	0.089	0.149	0.047	0.029	0.008
	25	0.136	0.088	0.143	0.047	0.016	0.008
	30	0.073	0.087	0.137	0.047	0.015	0.008
	35	0.071	0.085	0.132	0.046	0.015	0.008
3	10	0.090	0.120	0.153	0.049	0.018	0.009
	15	0.087	0.117	0.148	0.049	0.017	0.009
	20	0.085	0.115	0.187	0.049	0.017	0.008
	25	0.082	0.112	0.181	0.048	0.017	0.008
	30	0.085	0.110	0.135	0.048	0.016	0.008
	35	0.078	0.108	0.131	0.048	0.016	0.008